Hydrol. Earth Syst. Sci. Discuss., 10, 13333–13361, 2013
www.hydrol-earth-syst-sci-discuss.net/10/13333/2013/
doi:10.5194/hessd-10-13333-2013

Hydrology and Earth System Sciences
Discussions
Open Access

Long-term precipitation forecast for drought relief using atmospheric circulation factors: a study on the Maharloo Basin in Iran

S. K. Sigaroodi[1,2], Q. Chen[1,3], S. Ebrahimi[4], A. Nazari[2], and B. Choobin[2]

[1]RCEES Chinese Academy of Sciences, Beijing, 100085, China
[2]University of Tehran, Natural Resources Faculty, Karaj, Iran
[3]Nanjing Hydraulics Research Institute, Nanjing, 210023, China
[4]ITP Chinese Academy of Sciences, Beijing 100101, China

Received: 19 September 2013 – Accepted: 17 October 2013 – Published: 5 November 2013

Correspondence to: Q. Chen (qchen@rcees.ac.cn)

Published by Copernicus Publications on behalf of the European Geosciences Union.

Abstract

Long-term precipitation forecasts can help to reduce drought risk through proper management of water resources. This study took the saline Maharloo Lake, which is located in the south of Iran and is continuously suffering from drought disaster, as a case to investigated the relationships between climatic indices and precipitation. Cross correlation in combination with stepwise regression technique were used to determine the best variables among 40 indices and identify the proper time-lag between dependent and independent variables for each month. The monthly precipitation was predicted using Artificial Neural Network (ANN) and multi- regression stepwise methods, and results were compared with observed rainfall data. According to R^2, root mean square error (RMSE) and Nash–Sutcliffe factors, the ANN model performed better than the multi-regression model, which was also confirmed by classification results. Prediction accuracy was higher in the dry season (June to October) than in the other seasons. The highest and lowest accuracy of the ANN model were in September and March, respectively. Based on this research, the monthly precipitation anomalies in the Maharloo Basin in north of Persian Gulf can be forecast about ten months earlier using NOAA (National Oceanic and Atmospheric Administration) climate indices such as NAO (North Atlantic Oscillation), PNA (Pacific North America) and Nino, which will support drought-risk alleviation in the region.

1 Introduction

Arid and semi-arid climates cover over one quarter of the land area of the Earth and experience serious water scarcity, more than any other climate region. Drought has tremendous social and economic impacts on all over the world. The cost incurred by drought in Iran alone is estimated to be about USD 2 to 5 billion annually. It is therefore essential to have a proactive approach to reduce the impacts of the drought.

HESSD
10, 13333–13361, 2013

Precipitation forecasting is an important way to support water resources management so as to mitigate the harmful effects of droughts and climate change.

Short-term weather forecasting is mostly based on radar and satellite information analysis. Long-term prediction fills the gap between short-range weather forecasting and climate prediction, and points to timescales of more than one month to one year (Tourigny and Jones, 2009). The main source for the predictability results from large-scale atmospheric circulation anomalies due to tropical sea surface temperature (SST) anomalies (Teschl and Randeu, 2006). Sea surface temperature anomalies have relatively slow timescales, and may be predictable at a useful level of skill up to a season or a year (Shukla et al., 1998).

Many studies have investigated the relationship between SST anomalies and climatic phenomena variations, especially precipitation. Previous studies have demonstrated the influence of the El Niño/La Niña-Southern Oscillation (ENSO) on different climates since the 1980s (Vautard and Legras, 1988; Barnston et al., 1987; Fraedrich, 1994). Ferranti et al. (1990) and Flateau et al. (1997) studied the significant impact of the Madden–Julian Oscillation (MJO) on the speed of propagation in equatorial Indian and western Pacific oceans. Palmer et al. (2004) studied precipitation forecasting in autumn over the Mediterranean coast. Bladé et al. (2012) found high uncertainty on summer rainfall forecasts using the Summer North Atlantic Oscillation (SNAO) in Europe and Mediterranean, showing that the Mediterranean region was anomalously wet during high SNAO summers when strong anticyclonic conditions and suppressed precipitation overcame the United Kingdom. Guérémy et al. (2012) forecast French Mediterranean heavy precipitation events using weather regimes during autumn, and established an atmospheric link between Pacific SST anomalies and precipitation over this area.

Long-term predictions often exhibit high uncertainties. Scientists have made considerable effort to achieve greater accuracy and reliability through easily used methods and available data (Wu et al., 2011). To improve forecast accuracy, some researchers have attempted to discover nonlinear relationships between climatic phenomena and climatic indices patterns (Kim and Barros, 2001; Tourigny and Jones, 2009; Gueremy

HESSD
10, 13333–13361, 2013

et al., 2012). Li et al. (2012) applied the back-propagation method and identified five key indices out of 24 factors as the most effective variables in runoff forecasting during the flood season in the Nenjiang River Basin in China.

The present study investigated Maharloo Lake in Iran to explore more accurate long-term precipitation forecasting using multi-regression analysis and artificial neural network methods. The key contribution was the establishment of a ten-month-ahead precipitation forecasting model to support drought-risk management, and the applicability of the ANN model in long-term prediction using atmospheric circulation factors.

2 Materials and methods

2.1 Study area

Maharloo Lake (Fig. 1) is a saline shallow lake located 200 km north of the Persian Gulf in southern Iran. The lake covers an area of about 250 km^2, and the basin area is about 31 500 km^2. It is so salty that some areas are salt-mined during the dry season. The area is situated in an arid and semi-arid region. Rainfall varies from 150 mm on the plains to 650 mm on the high mountains, with an average of 350 mm. The lake is recharged by two seasonal rivers, the Soltan Abad and Khoshk.

During winter, several migratory bird species from northern Russia, including flamingos (*Phoenicopterus roseus*), common shelducks (*Tadorna tadorna*) and mallards (*Anas platyrhynchos*), spend four months in the area feeding on brine shrimp (*Artemia franciscana*). Thus, the lake has important ecological value.

Recently the lake water has decreased, especially during drought episodes. In 2008, about 90 % of Maharloo Lake dried out, which caused the number of flamingos to decrease from 150 000 to only 5000 (ISNA Press, 2008). In addition, the lake watershed is used for agricultural and industrial activities that consume a large portion of water. Therefore, long-term prediction of precipitation can help adjust agricultural and industrial activities and consider lake sustainability based on ecological water rights.

HESSD
10, 13333–13361, 2013

The climate of the area is affected by different systems, including the Mediterranean and Black Sea from the west, the Caspian Sea from the north, and the Persian Gulf and Arabian Sea from the south, which add to the difficulty and uncertainty in precipitation prediction.

2.2 Precipitation data

Precipitation data from four gauges (Shiraz, Dehkade, Ali Abad and Dashtbal) located in Mharloo basin during January 1967 to December 2009 is used. Time series of monthly precipitation values obtained from these gauges and the Thiessen method were used to calculate the mean monthly precipitation series for the entire basin.

2.3 Atmospheric circulation factors

Atmospheric dynamics are influenced by solar activity through solar sunspots activity and radiation intensity. Sunspots are temporary phenomena on the photosphere of the Sun that appear visibly as dark spots compared to surrounding regions. Solar radiation intensity is the energy source for climatic systems and is a relatively stable influence, so is generally considered as a constant factor. However, sunspot cycles approximately 11 yr. Sunspots number is correlated with precipitation and drought. Wang et al. (1997) studied the relationship between relative sunspot number and runoff in the Huanghe River Basin. Christensen et al. (1991) and Weickmann et al. (2000) found that sunspot cycle length showed good correlation with Northern Hemisphere land temperature and drought periods.

The specific heat and mass of the water on Earth are large (Li, 2012). The huge heat capacity of the oceans brings an obvious and long-term effect to atmosphere-ocean interactions, which affects atmospheric circulation in subsequent periods. Atmospheric circulation factors represent the physical properties correlated with precipitation. In this study, 40 climate indices from the NOAA website (http://www.esrl.noaa.gov/gmd/dv/ftpdata.html) were used. Table 1 lists the climatic indices selected as atmospheric circulation predictors and their recorded period.

2.4 Description of methods

Since large differences existed in the means and variations between the parameters, the data were normalized (Trenberth, 1994; Teschl, 2006; Guérémy, 2012) before they were used in the model. After normalization, each time series of monthly rainfall and climate indices were in the range of 0 and 1 (see Appendix: Eq. 1).

2.4.1 Multivariate regression

The time-lag between dependent and independent variables was different for each input variable. Cross correlation was used to find the proper independent variables and identify their time lags. The final multivariate equation was determined using the stepwise method. The stepwise regression method selects the predictive variables by an automatic procedure starting with the best-correlated variable. It adds the variable (if any) if the addition of this variable significantly improves model performance. This process repeats until no improvement is obtained (Prasad, 2010).

2.4.2 Artificial neural network

The application of ANN in hydrology forecasting started in the early 1990s, covering rainfall–runoff modeling (Fernando et al., 1998), stream flow forecasting (Kim and Barros, 2001) and groundwater level forecasting (Coulibaly et al., 2001).

The ANN usually consists of an input, hidden and output layer. Multi-layer perceptron (MLP) is the most widely used ANN in forecasting models, and was applied in this study. The same independent variables of the multivariate regression model were used as the input. The data set was divided into two groups, 80 % was used for model training and 20 % was used for cross validation. For each month, neural network training and validation were repeated 20 times and the best result was selected according to R^2 and root mean squared error (RMSE).

2.5 Evaluation criteria

The R^2 and RMSE between model outputs and observations were used as the primary indicators of model performance. The higher the R^2 value and the smaller the RMSE, the better were the model results. Other criteria including Nash–Sutcliffe efficiency, accuracy percentage, Heidke skill score, trend accuracy and Taylor diagrams were used to further quantify forecasting accuracies (see Appendix: Eqs. 2–5).

Nash–Sutcliffe efficiency ranges from $-\infty$ to 1, and a value higher than 0 means model predictions were better than the mean of observations.

Accuracy percentage shows what fraction of the forecasts is in the correct category, and it ranges between 0 and 1. To calculate this value, monthly precipitations were categorized into five classes (very dry, dry, normal, wet and very wet) based on SPI factor (see Appendix: Table A1).

Heidke skill score (HSS) indicates the fraction of correct forecasts after eliminating randomly correct forecasts since some forecasts can be correct due purely to random chance.

Trend accuracy gives the percentage for which the actual output changes in the correct direction relative to the previous desired value. Trend accuracy measures the proportion of the trend that has been correctly predicted. In this case, the trend is either “up” or “down”.

Taylor diagrams provide a statistical summary of how well modeled patterns match observed patterns in terms of correlation, RMSE and variance.

HESSD
10, 13333–13361, 2013

3 Results

3.1 Regression results

For each independent variable, the best time-lag to the dependent variable was determined through cross correlation. Table 2 shows the correlation between the PNA index and precipitation in different time-lag months. For example, the best time-lag to predict precipitation in January using the PNA index was five months (the previous August). It is seen that for different month, the best time-lag is different.

Table 3 shows the top 10 factors out of 40 indices and the corresponding best time-lags. They were ranked by R^2, and only the R^2 that is higher than 0.05 were listed. The indices in the first line of the table are the best indices to predict monthly precipitation for univariate regression. These indices explained less than 25 % (mostly less than 20 %) of total variation, and such low values of R^2 implied that precipitation in the area was not affected by one particular region only with a constant interval.

To improve model performance, more independent variables were added via the stepwise regression method. Tables 4–6 show the results of the correlation matrix, ANOVA table, and multivariate coefficients for January precipitation, respectively.

It is seen from Table 4, the precipitation in January P(Jan) has significant correlation with PNA, QBO and TNA. Also, there is a strong correlation between PNA and TNA. Given the fact that the correlation between P(Jan) and PNA is higher than the correlation between P(Jan) and TNA, TNA was ruled out while PNA and QBO were finally selected as the independent variables for predicting the precipitation in January, as proved by Tables 5 and 6.

Similarly, the procedures were applied to all the other months. The final selected independent variables are listed in parentheses in Table 3, and Table 7 presents the univariate and multivariate regression results for an entire year.

Results showed that R^2 increased and the regressions explained up to 44 % (mostly more than 30 %) of total variation. For July and September, only univariate regression

HESSD
10, 13333–13361, 2013

was selected because adding more variables did not make improvement to the prediction.

3.2 ANN results

Since a neural network can arrive at different solutions for the same data due to initialization of network weights, results from 20 repetitions for each month were selected. The results showed that the ANN model explained more than 40 % (up to 76 %) of total variation. Figure 2 presents comparisons between the ANN model results and the observations. Although the ANN model results were better than the regression model results, both methods failed to predict some extreme values.

3.3 Results evaluation

Table 8 presents the precipitation classification results of the ANN and regression models, and Table 9 gives the R^2, RMSE, Nash–Sutcliffe, trend accuracy and Heidke skill score values. The values of R^2, RMSE, Nash–Sutcliffe, trend accuracy and Heidke skill score were higher when the time-lag was ten months. In general, the ANN model performed better than the regression model. Trend accuracy determines the accuracy of variation direction, and was almost equal in both methods. However, this criterion is sensitive to false prediction, thus even one false prediction can decrease its value seriously. For example, the false prediction of February precipitation in 1999 using the ANN method caused a decrease in trend accuracy, even though the other evaluation criteria were better.

Taylor diagrams can highlight the goodness of different models compared to observations. The diagram can be visualized as a series of points on a polar plot. The azimuth angle refers to the correlation coefficient between the predicted and observed data. Radial distance from the origin represents the ratio of the normalized standard deviation (SD) of the simulation to that of the observation. The distance from the reference point (observations) is a measure of the centered RMSE (Taylor, 2001, 2005).

Therefore, an ideal model (being in full agreement with the observations) is marked by the reference point with the correlation coefficient equal to 1, and the same amplitude of variations compared with the observations (Heo, 2013). Figure 3 displays the normalized standard deviation (SD) and correlation coefficient R^2 of the ANN and regression models. The ANN results were closer to the observation points than were the regression results. In the diagram, the SD of all predicted data of both methods were less than the observations, indicating that neither method well-captured the fluctuation of the natural events.

4 Discussion and conclusions

The Maharloo watershed is suffering from water scarcity, while the watershed is dominated by agricultural and industrial activities that demand a large amount of water. Therefore, long-term prediction of precipitation can help adjusting agricultural and other activities and consider lake sustainability based on ecological water requirements, especially during drought period when the ecosystem is more frangible.

The present study applied multivariate regression and ANN methods for the long-term prediction of precipitation in the Maharloo Lake Basin in Iran. It used atmospheric circulation factors and cross correlation to identify proper independent variables and time-lags, among 40 indices and 12 months delay for each target month. The monthly precipitation was predicted and compared with the measured data.

The NAO, PNA and QBO indices were more frequently used than the other indices, indicating that the regional precipitation of the Maharloo Basin was mainly affected by the North Atlantic oscillation and the Pacific North American. These results agree with Guérémy et al. (2012) who discussed the link between Pacific SST anomalies and precipitation over the Mediterranean region. Therefore, the Pacific SST anomalies can affect the Mediterranean region as well as southern Iran. The higher rates of observed precipitation variation compared with the modeled predictions implied that other regional conditions (such as temporal wind and local humidity) also affected and complicated the precipitation system.

Generally, the predicted results in dry months (June to October) were better than other months. This is also indicated in Fig. 2 that the rainfall peaks are mostly not well predicted, while the drought (low rainfall) are well captured by both methods.

Detailed comparison of numerical values is usually not straightforward, thus comparing the precipitation classes make it easier to evaluate the different techniques. As shown in Table 8, the performance of ANN is mostly better than the regression method. Also in Table 9, Heidke Skill Scores can more clearly quantify the performance difference between ANN and regression methods than other indicators. The Maharloo Lake Basin is usually lacking of rainfall in summer, thus the five classes decreased to three classes (normal, dry and very dry). Consequently, the results of trend accuracy and Heidke Skill Score related to these classes were significantly higher than other months.

The better results of the ANN model compared to the regression model on the relationships between atmospheric indices and regional precipitation showed the high flexibility of the ANN method and the nonlinear nature of the relationships. These results were consistent with the findings of previous studies (Teschl and Randeu, 2006; Li et al., 2012; Wu, 2010), which showed the ability of the ANN model to determine an atmospheric link between SST anomalies and precipitation over the inland area of the Persian Gulf.

In general, due to large spatial-temporal distance between climatic indices and precipitation in destination as well as the coarse resolution of the data, the accuracy of the models were relatively low, which was also pointed by some other scientists (Ferranti, 1990; Fernando, 1998; Palmer, 2004; Gueremy, 2012).

Future study should determine how different indices affect regional precipitation, whether the results are extendable to a larger area, and whether global changes such as global warming are influential in source or destination areas.

Appendix A

Normalization function

$$X_{\text{norm}} = \frac{X_i - X_{\min}}{X_{\text{Max}} - X_{\min}} \tag{A1}$$

where X_{norm} is the normalized value of X_i and X_{Max} and $X_{\min}$ are the maximum and minimum of the data series, respectively (range: 0 to 1).

Appendix B

Root Mean Square Error (RMSE)

$$\text{RMSE} = \sqrt{\frac{\sum_{i=1}^{n}(X_{\text{O}} - X_{\text{E}})^2}{n}} \tag{B1}$$

where X_{O} and X_{E} are the observed and estimated values, respectively (range: 0 to ∞, perfect value: 0).

Appendix C

Standardized Precipitation Index (SPI) and categorization

$$\text{SPI} = \frac{P_i - \overline{P}}{\text{SD}} \cdot 100 \tag{C1}$$

where P_i is the precipitation, $\overline{P}$ and SD are the mean and standard deviation of the precipitation, respectively. SPI is categorized using the following table (Table A1).

HESSD
10, 13333–13361, 2013

Appendix D

Accuracy and Heidke skill score (HSS)

$$\text{Accuracy} = \frac{1}{N}\sum_{i=1}^{k} n(F_i \cdot O_i) \quad \text{(D1)}$$

$$\text{HSS} = \frac{\frac{1}{N}\sum_{i=1}^{k} n(F_i \cdot O_i) - \frac{1}{N}\sum_{i=1}^{k} n(F_i)n(O_i)}{1 - \frac{1}{N^2}\sum_{i=1}^{k} n(F_i)n(O_i)} \quad \text{(D2)}$$

in these formulas $n(F_i \cdot O_i)$ denotes the number of forecasts in category i that had observations in same category; $n(F_i)$ and $n(O_i)$ denote the total number of forecasts and observations in category I; and N is the total number of forecasts. (Accuracy range: 0 to 1, perfect value is 1; HSS range: $-\infty$ to 1, 0 indicates no skill, perfect score is 1.)

Supplementary material related to this article is available online at http://www.hydrol-earth-syst-sci-discuss.net/10/13333/2013/hessd-10-13333-2013-supplement.pdf.

Acknowledgements. This research was supported by the National Natural Science Foundation of China (50920105907, 51279196) and the National Basic Research Program 973 (No. 2010CB429004).

References

Barnston, A. G. and Livezey, R. E.: Classification, seasonality and persistence of low-frequency atmospheric circulation patterns, Mon. Weather Rev., 115, 1083–1126, 1987.

HESSD
10, 13333–13361, 2013
Drought forecasting by atmospheric circulation factors
S. K. Sigaroodi et al.

Blade, I., Liebmann, B., and Fortuny, D.: Observed and simulated impacts of the summer NAO in Europe: implications for projected drying in the Mediterranean region, Clim. Dynam., 39, 709–727, 2012.
Coulibaly, P., Anctil, F., Aravena, R., and Bobée, B.: Artificial neural network modeling of water table depth fluctuations, Water Resour. Res., 37, 885–896, 2001.
Fernando, D. A. K. and Jayawardena, A. W.: Runoff forecasting using RBF networks with OLS algorithm, J. Hydrol. Eng., 3, 203–209, 1998.
Ferranti, L., Palmer, T. N., Molteni, F., and Klinker, E.: Tropical-extratropical interaction associated with the 30–60 day oscillation and its impact on medium and extended range prediction, J. Atmos. Sci., 47, 2177–2199, 1990.
Fraedrich, K.: An ENSO impact on Europe?, Tellus A, 46, 541–552, 1994.
Friis-Christensen, E. and Lassen, K.: Length of the solar cycle: an indicator of solar activity closely associated with climate, Science, 254, 698–700, 1991.
Guérémy, J.-F., Laanaia, N., and Céron, J.-P.: Seasonal forecast of French Mediterranean heavy precipitating events linked to weather regimes, Nat. Hazards Earth Syst. Sci., 12, 2389–2398, doi:10.5194/nhess-12-2389-2012, 2012.
Heo, K. Y., Ha, K. J., Yun, K. S., Lee, S. S., Kim, H. J., and Wang, B.: Methods for uncertainty assessment of climate models and model predictions over East Asia, Int. J. Climatol., 1–14, doi:10.1002/joc.3692, 2013.
ISNA Press, available at: http://isna.ir/fa/imageReport/91040502289 (last access: 3 November 2013), 2008.
Kim, G. and Barros, A. P.: Quantitative flood forecasting using multisensor data and neural networks, J. Hydrol., 246, 45–62, 2001.
Li, H., Xie, M., and Jiang, S.: Recognition method for mid- to long-term runoff forecasting factors based on global sensitivity analysis in the Nenjiang River Basin, Hydrol. Process., 26, 2827–2837, 2012.
Maria, F., Flatau, P. J., Phoebus, P., and Niiler, P. P.: The feedback between equatorial convection and local radiative and evaporative processes: the implications for intraseasonal oscillations, J. Atmos. Sci., 54, 2373–2386, 1997.
Palmer, T., Andersen, U., Cantelaube, P., Davey, M., Deque, M., Doblas-Reyes, F. J., Feddersen, H., Graham, R., Gualdi, S., Gueremy, J. F., Hagedorn, R., Hoshen, M., Keenlyside, N., Latif, M., Lazar, A., Maisonnave, E., Marletto, V., Morse, A. P., Orfila, B., Rogel, P., Terres, J. M., and Thomsen, M. C.: Development of a European multi-model ensemble system

for seasonal to inter-Annual prediction (DEMETER), B. Am. Meteorol. Soc., 85, 853–872, 2004.
Penland, C. and Matrosova, L.: Prediction of tropical Atlantic sea surface temperatures using linear inverse modeling, J. Climate, 11, 483–496, 1998.
Prasad, K., Dash, S. K., and Mohanty, U. C.: A logistic regression approach for monthly rainfall forecasts in meteorological subdivisions of India based on DEMETER retrospective forecasts, Int. J. Climatol., 30, 1577–1588, 2010.
Shukla, J., Anderson, J., Baumhefner, D., Brankovic, C., and Chang, Y.: Dynamical seasonal prediction, B. Am. Meteorol. Soc., 81, 2593–2606, 2000.
Taylor, K. E.: Summarizing multiple aspects of model performance in a single diagram, J. Geophys. Res., 106, 7183–7192, 2001.
Taylor, K. E.: Taylor Diagram Primer, available at: http://www-pcmdi.llnl.gov/about/staff/Taylor/CV/Taylor_diagram_primer.pdf (last access: 3 November 2013), 2005.
Teschl, R. and Randeu, W. L.: A neural network model for short term river flow prediction, Nat. Hazards Earth Syst. Sci., 6, 629–635, doi:10.5194/nhess-6-629-2006, 2006.
Tourigny, E. and Jones, C. G.: An analysis of regional climate model performance over the tropical Americas, Part 1 and 2: Simulating seasonal variability of precipitation associated with ENSO forcing, Tellus A, 61, 323–356, 2009.
Trenberth, H.: Decadal atmosphere-ocean variations in the Pacific, Clim. Dynam., 9, 303–319, 1994.
Vautard, R. and Legras, B.: On the source of mid latitude low frequency variability, Part 2: Nonlinear equilibration of weather regimes, J. Atmos. Sci., 45, 2845–2867, 1988.
Wang, W., Van Gelder, P. H. A. J. M., Vrijling, J. K., and Ma, J.: Forecasting daily streamflow using hybrid ANN models, J. Hydrol., 324, 383–399, 2006.
Wang, Y., Xue, Y., Peng, Z., and Wang, G.: The relationship between the solar activity and runoff and floods of the Yellow River, Water Resources and Water Engineering, 8, 30–43, 1997.
Wu, C. L. and Chau, K. W.: Data-driven models for monthly stream flow time series prediction, Eng. Appl. Artif. Intel., 23, 1350–1367, 2010.
Wu, L., Seo, D. J., Demargne, J., Brown, J. D., Cong, S., and Schaake, J.: Generation of ensemble precipitation forecast from single-valued quantitative precipitation forecast for hydrologic ensemble prediction, J. Hydrol., 399, 281–298, 2011.

HESSD
10, 13333–13361, 2013

Title Page
Abstract | Introduction
Conclusions | References
Tables | Figures
◂◂ | ▸▸
◂ | ▸
Back | Close
Full Screen / Esc
Printer-friendly Version
Interactive Discussion

Table 1. Primary selection of atmospheric circulation predictors.

No	Climate Index	Data Period	No	Climate Index	Data Period
1	PNA	1950–2013	21	Hurricane Activity	1950–2009
2	EP/NP	1950–2013	22	AO	1950–2011
3	WP	1950–2013	23	Pacific Warm Pool	1948–2008
4	NAO	1950–2013	24	CAR	1951–2010
5	NAO (Jones)	1948–2001	25	QBO	1948–2013
6	SOI	1951–2013	26	AMM	1948–2013
7	Nino 3	1950–2013	27	NTA	1951–2010
8	BEST	1948–2011	28	Atlantic Multi Decadal Oscillation Smoothed	1948–2007
9	TNA	1948–2013	29	Globally Integrated Angular Momentum	1958–2013
10	TSA	1948–2013	30	ENSO Precipitation Index	1979–2009
11	WHWP	1948–2013	31	Central Indian Precipitation (monsoon)	1948–1999
12	ONI	1950–2013	32	Sahel Rainfall	1948–2001
13	MEI	1950–2013	33	SW Monsoon Region Rainfall	1948–2010
14	Nino 1+2	1950–2013	34	Northeast Brazil Rainfall Anomaly	1948–2000
15	Nino 4	1950–2013	35	Solar Flux (10.7 cm)	1948–2013
16	Nino 3.4	1950–2013	36	Global Mean Land/Ocean Temperature Index	1948–2013
17	PDO	1948–2013	37	Atlantic Multi Decadal Oscillation Unsmoothed	1948–2013
18	NOI	1948–2007	38	Tropical Pacific SST EOF	1948–2008
19	NP	1948–2011	39	Atlantic Triple SST EOF	1948–2008
20	TNI	1948–2013	40	Sunspot	1749–2013

HESSD
10, 13333–13361, 2013

Table 2. Cross correlation between PNA index and precipitation.

Delay	Jan	Feb	Mar	Apr	May	Jun	Jul	Aug	Sep	Oct	Nov	Dec
+12 month	0.024	0.005	0.001	0.051	0.006	0.082	0.038	0.001	0.001	0.004	0.010	0.029
+11 month	0.021	0.005	0.006	0.008	0.003	0.155[b]	0.003	0.075	0.000	0.040	0.000	0.033
+10 month	0.001	0.009	0.042	0.056	0.000	0.029	0.001	0.000	0.000	0.002	0.011	0.012
+9 month	0.002	0.000	0.013	0.001	0.003	0.033	0.019	0.005	0.006	0.009	0.003	0.002
+8 month	0.053	0.005	0.001	0.008	0.039	0.004	0.001	0.039	0.007	0.018	0.028	0.002
+7 month	0.005	0.001	0.086	0.010	0.001	0.014	0.002	0.002	0.011	0.038	0.054	0.032
+6 month	0.013	0.064	0.016	0.004	0.028	0.009	0.000	0.062	0.001	0.004	0.000	0.020
+5 month	0.117[a]	0.032	0.027	0.038	0.008	0.014	0.004	0.001	0.024	0.007	0.012	0.012
+4 month	0.011	0.004	0.016	0.000	0.000	0.022	0.005	0.004	0.024	0.029	0.110[a]	0.000
+3 month	0.014	0.003	0.024	0.037	0.049	0.005	0.018	0.000	0.085	0.010	0.025	0.007
+2 month	0.001	0.005	0.003	0.004	0.024	0.000	0.000	0.115[a]	0.000	0.104[a]	0.004	0.000
+1 month	0.072	0.001	0.005	0.066	0.000	0.011	0.002	0.060	0.013	0.002	0.008	0.008

[a] Correlation is significant at the 0.05 level.
[b] Correlation is significant at the 0.01 level.

HESSD
10, 13333–13361, 2013

Table 3. Ranked indices and proper time-lags for each month of a year.

Ranking	Factor	Jan	Feb	Mar	Apr	May	Jun	Jul	Aug	Sep	Oct	Nov	Dec
1st	R^2	0.117	0.142	0.263	0.212	0.209	0.195	0.236	0.144	0.155	0.151	0.182	0.117
	Single	(PNA)	(QBO)	(GIAM)	(NAO)	(Alt, Tro, SST)	(SWMRR)	(Alt, Me, Mo)	(QBO)	(NAO)	(SOI)	(Nino1+2)	(SWMRR)
	Time-lag	5	11	9	11	8	7	10	1	10	3	8	8
2nd	R^2	0.115	0.131	0.152	0.153	0.171	0.155	0.164	0.122	0.116	0.132	0.171	0.107
	Single	(QBO)	NAO	PDO	Nino3	TNA	PNA	CAR	EP, NP	AO	(BEST)	(TSA)	TNI
	Time-lag	10	7	6	12	8	11	12	7	3	3	4	4
3rd	R^2	0.106	0.109	0.122	0.139	0.153	0.148	0.163	0.122		0.105	0.123	0.099
	Single	TNA	SOI	SWMRR	Nino1+2	Alt, Me, Mo	(AO)	NTA	(AO)		AO	AO	(TNA)
	Time-lag	1	11	6	12	9	12	11	4		9	8	7
4th	R^2		0.102	0.109	0.133	0.152	0.098	0.153	0.115		0.104	0.11	0.096
	Single		BEST	Nino1+2	NP	Long, AMO	WP	SWMRR	PNA		PNA	PNA	NTA
	Time-lag		11	10	1	7	11	9	2		2	4	8
5th	R^2		0.097	0.108	0.128	0.152		0.127	0.099		0.095	0.105	0.094
	Single		(WHWP)	TNI	(GIAM)	Alt, Mul. Osc		Alt, Tro, SST	WP		WP	SWMRR	SOI
	Time-lag		2	7	11	7		7	9		1	11	1
6th	R^2		0.096	0.106	0.118	0.15		0.124	0.098		0.093	0.097	
	Single		EP, NP	QBO	Tro, Pac, SST	AO		TNA	PDO		QBO	WP	
	Time-lag		10	8	12	12		10	3		7	3	
7th	R^2			0.103	0.116	0.14		0.12				0.095	
	Single			(NAO)	WHWP	GMLOT		EP, NP				EP, NP	
	Time-lag			7	11	5		11				10	
8th	R^2			0.1	0.112	0.128		0.118				0.093	
	Single			HURR	Solar	WP		Long, AMO				Pac WP	
	Time-lag			5	9	8		12				2	
9th	R^2				0.097	0.109		0.118					
	Single				SWMRR	(NAO)		Alt, Mul, Osc					
	Time-lag				1	10		12					
10th	R^2				0.095	0.106		0.11					
	Single				Nino3.4	WHWP		Pac WP					
	Time-lag				12	7		12					

HESSD
10, 13333–13361, 2013

Title Page
Abstract | Introduction
Conclusions | References
Tables | Figures
◀| |▶
◀ ▶
Back | Close
Full Screen / Esc
Printer-friendly Version
Interactive Discussion

Table 4. Correlation matrix between Jan precipitation and selected indices.

		P(Jan)	PNA	QBO	TNA
P(Jan)	Pearson Correlation	1	0.34*	−0.34*	0.33*
	Sig. (2-tailed)		0.03	0.03	0.03
	N	43	43	43	43
PNA	Pearson Correlation	0.34*	1	−0.06	0.26
	Sig. (2-tailed)	0.03		0.69	0.01
	N	43	43	43	43
QBO	Pearson Correlation	–.034*	−0.06	1	−0.09
	Sig. (2-tailed)	0.03	0.69		0.58
	N	43	43	43	43
TNA	Pearson Correlation	0.33*	0.26	−0.09	1
	Sig. (2-tailed)	0.03	0.10	0.58	
	N	43	43	43	43

* Significant correlation.

HESSD

10, 13333–13361, 2013

Drought forecasting by atmospheric circulation factors

S. K. Sigaroodi et al.

Table 5. ANOVA analyses for the regressions of precipitation in January.

Model[a]		Sum of Squares	d*f*	Mean Square	*F*	Sig.
1	Regression	0.21	1	0.21	5.35	0.026
	Residual	1.61	41	0.04		
	Total	1.82	42			
2	Regression	0.40	2	0.20	5.54	0.008
	Residual	1.43	40	0.04		
	Total	1.82	42			

[a] Dependent variable *P*(Jan);
Model 1: Independent variable PNA;
Model 2: Independent variables PNA and QBO.

HESSD
10, 13333–13361, 2013
Drought forecasting by atmospheric circulation factors
S. K. Sigaroodi et al.

HESSD
10, 13333–13361, 2013

Drought forecasting by atmospheric circulation factors

S. K. Sigaroodi et al.

Table 6. Coefficients of univariate and multivariate regression models.

Model[a]		Unstandardized coefficients		Standardized coefficients	*t*	Sig.
		B	Std. Error	Beta		
1	Constant	0.168	0.065		2.580	0.014
	PNA	0.286	0.124	0.340	2.313	0.026
2	Constant	0.318	0.091		3.513	0.001
	PNA	0.269	0.118	0.0320	2.282	0.028
	QBO	−0.234	0.103	−0.319	−2.276	0.028

[a] Dependent variable *P*(Jan);
Model 1: Independent variable PNA;
Model 2: Independent variables PNA and QBO.

Table 7. Univariate and multivariate regression models for each month of a year.

Month	Formula	R^2	N	Sig.
Jan	$NP = 0.286(PNA_5)+0.168$	0.12	43	5 %
	$NP = 0.269(PNA_5)-0.234(QBO_{10})+0.318$	0.22	43	1 %
Feb	$NP = -0.359(QBO_{11})+0.532$	0.14	43	5 %
	$NP = -0.364(QBO_{11})+0.552(WHWP_2)+0.485$	0.25	43	1 %
Mar	$NP = 0.559(GIAM_9)+0.115$	0.26	43	1 %
	$NP = 0.529(GIAM_9)+0.278(NAO_7)-0.028$	0.34	43	1 %
Apr	$NP = -0.492(NAO_{11})+0.510$	0.21	43	1 %
	$NP = -0.533(NAO_{11})-0.412(GIAM_{11})+0.713$	0.39	43	1 %
May	$NP = -0.540(\text{Atl-Tro-SST}_8)+0.454$	0.21	43	1 %
	$NP = -0.573(\text{Atl-Tro-SST}_8)-0.538(NAO_{10})+0.816$	0.37	43	1 %
Jun	$NP = 0.502(SWMRR_7)-0.073$	0.20	43	1 %
	$NP = 0.538(SWMRR_7)+0.474(AO_{12})-0.314$	0.44	43	1 %
Jul	$NP = -0.508(\text{Atl-MM}_{10})+0.325$	0.30	43	1 %
Aug	$NP = -0.239(QBO_1)+0.206$	0.15	43	5 %
	$NP = -0.247(QBO_1)-0.356(AO_4)+0.396$	0.36	43	1 %
Sep	$NP = 0.328(NAO_{10})-0.090$	0.18	43	1 %
Oct	$NP = -0.355(SOI_3)+0.262$	0.15	43	1 %
	$NP = -0.360(SOI_3)+0.349(WP_1)+0.058$	0.28	43	1 %
Nov	$NP = -0.511(\text{Nino1+2}_8)+0.386$	0.18	43	1 %
	$NP = -0.432(\text{Nino1+2}_8)-0.313(TSA_4)+0.518$	0.33	43	1 %
Dec	$NP = 0.357(SWMRR_8)+0.184$	0.12	43	5 %
	$NP = 0.415(SWMRR_8)-0.419(TNA_7)+0.338$	0.26	43	1 %

Note: Subscript numbers presents time-lags in a month. NP: Normalized Precipitation, PNA: Pacific North American, QBO: Quasi-Biennial Oscillation, GIAM: Globally Integrated Angular Momentum, NAO: North Atlantic Oscillation, Atl-Tro-SST: Atlantic Tripole SST, SWMRR: SW Monsoon Region rainfall, Atl-MM: Atlantic Meridional Mode, SOI: Southern Oscillation Index, Nino1+2: Extreme Eastern Tropical Pacific SST, WHWP: Western Hemisphere warm pool, AO: Antarctic Oscillation, BEST: Bivariate ENSO Time series, TSA: Tropical Southern Atlantic, TNA: Tropical Northern Atlantic.

HESSD
10, 13333–13361, 2013

Table 8. Precipitation classes predicted by regression model and ANN model and their comparisons with observations.

Year	Jan			Feb			Mar			Apr			May			Jun		
	Ob	Re	NN	Ob	Re	NN	Ob	Re	NN	Ob	Re	NN	Ob	Re	NN	Ob	Re	NN
1967	N	W	VW	W	N	N	VP	D	N	W	N	N	N	N	N	N	N	N
1968	D	N	D	N	D	N	W	N	N	VW	W	VW	D	N	N	N	N	N
1969	VW	W	VW	D	N	N	N	D	N	VW	VW	VW	VW	W	N	N	N	N
1970	N	N	N	D	N	N	D	N	N	D	D	D	D	N	N	N	N	N
1971	D	N	N	N	N	N	VP	D	D	N	N	D	D	N	N	N	N	N
1972	N	N	N	N	N	N	VW	N	N	N	N	N	N	N	W	N	N	N
1973	N	N	D	D	N	N	N	W	N	D	D	D	D	N	W	N	N	N
1974	W	N	N	N	N	N	N	N	N	N	N	W	N	N	N	N	N	N
1975	N	N	W	N	N	N	N	D	N	VW	N	W	VW	VW	VW	N	N	N
1976	N	N	N	VW	N	VW	VW	D	N	W	W	N	N	N	N	N	N	N
1977	D	D	D	D	D	N	D	W	N	W	N	D	N	N	N	N	N	N
1978	VW	VW	VW	N	W	N	N	D	D	N	W	W	D	W	N	N	N	N
1979	W	N	N	D	N	D	N	N	N	D	D	D	W	W	N	VW	VW	VW
1980	N	N	N	W	N	N	W	W	W	D	N	N	D	N	N	N	N	N
1981	N	D	N	N	N	N	N	N	N	N	W	W	W	W	N	N	N	N
1982	N	D	N	N	N	N	VW	N	N	D	D	N	N	N	N	N	N	N
1983	N	W	N	N	W	VW	N	W	W	D	N	N	N	N	N	N	N	N
1984	VP	N	N	D	N	N	VW	VW	W	D	D	D	VW	N	N	N	N	N
1985	W	N	N	N	N	N	VP	D	VP	VP	N	N	N	N	N	N	N	VW
1986	VP	N	N	D	N	N	N	N	N	W	N	VW	VW	N	N	N	N	N
1987	VP	D	N	D	N	N	W	N	N	N	N	D	D	N	N	N	VW	N
1988	W	W	N	VW	W	W	N	N	N	N	D	D	D	N	D	N	N	N
1989	VP	N	N	N	N	N	D	N	N	N	D	N	N	N	N	N	N	N
1990	N	N	N	VW	N	N	VP	N	N	N	N	D	D	N	N	N	N	N
1991	VW	W	VW	N	N	N	W	W	N	VP	N	N	D	N	D	N	N	N
1992	N	N	D	N	D	N	N	W	N	N	N	N	VW	N	N	N	N	N
1993	W	N	W	VW	W	W	VW	N	N	D	VP	D	D	W	W	N	N	N
1994	VP	N	D	VP	N	VP	W	W	W	D	N	N	VW	VW	N	N	N	N
1995	VP	N	N	VW	W	VW	D	N	N	VW	W	N	N	N	N	VW	VW	N
1996	W	N	D	N	N	N	VW	W	W	N	N	W	N	N	D	N	N	N
1997	D	N	N	VP	N	W	VW	N	N	VW	W	VW	N	D	N	N	N	N
1998	N	N	N	VW	VW	N	VW	VW	VW	N	D	N	N	D	N	N	N	N
1999	N	N	N	VW	N	N	N	N	N	D	N	D	D	N	D	N	N	N
2000	VW	N	W	VP	D	N	VP	N	N	VP	N	D	D	N	D	N	N	N
2001	VP	N	N	N	N	N	VP	D	D	VP	N	D	N	N	N	VW	W	VW
2002	W	W	VW	N	W	N	D	D	N	VW	W	N	D	D	D	N	N	N
2003	N	N	N	W	N	N	W	N	N	D	N	N	D	D	N	N	N	N
2004	VW	N	N	D	N	N	VP	N	N	N	N	N	N	D	D	N	N	N
2005	N	N	N	D	N	N	D	N	N	N	N	N	D	D	D	N	W	N
2006	N	N	N	N	N	N	VP	N	D	W	W	N	D	D	D	N	N	N
2007	D	N	N	N	N	N	VW	N	N	W	W	W	N	D	D	N	N	N
2008	N	W	N	VP	N	N	VP	D	D	VP	N	N	D	N	N	N	N	N
2009	VP	N	N	D	N	D	N	D	N	N	VW	W	N	N	D	N	N	N

Ob: Observed Re: Regression NN: Neural Network VW: Very Wet W: Wet N: Normal D: Dry VD: Very Dry.

HESSD
10, 13333–13361, 2013

Drought forecasting by atmospheric circulation factors

S. K. Sigaroodi et al.

Title Page
Abstract | Introduction
Conclusions | References
Tables | Figures
◀| |▶
◀ ▶
Back | Close
Full Screen / Esc
Printer-friendly Version
Interactive Discussion

Table 8. Continued.

Year	Jul			Aug			Sep			Oct			Nov			Dec		
	Ob	Re	NN	Ob	Re	NN	Ob	Re	NN	Ob	Re	NN	Ob	Re	NN	Ob	Re	NN
1967	N	N	N	N	N	N	N	N	N	N	N	N	VW	W	VW	D	N	N
1968	N	N	N	N	N	N	N	N	N	N	N	N	D	N	N	N	N	N
1969	N	N	N	N	N	N	N	N	N	N	N	N	N	N	N	D	D	N
1970	N	N	N	N	N	N	N	N	N	N	N	N	D	W	W	D	D	N
1971	N	N	N	N	N	N	N	N	N	N	N	N	N	W	VW	N	N	N
1972	N	N	N	N	N	N	N	N	N	N	N	N	D	N	D	D	N	N
1973	VW	VW	VW	N	N	N	N	N	N	N	N	N	D	N	D	D	N	N
1974	N	N	N	N	N	N	N	N	N	N	N	N	D	N	N	VW	N	N
1975	VW	VW	VW	N	N	N	N	N	N	N	N	N	N	N	N	N	W	N
1976	VW	N	N	N	N	N	N	N	N	VN	N	W	N	W	VW	N	W	N
1977	N	N	N	N	N	N	N	N	N	VW	VW	VW	W	N	N	W	N	N
1978	VW	N	N	N	N	N	N	N	N	N	N	N	VW	W	W	N	N	N
1979	N	N	N	VW	VW	VW	N	VW	W	N	N	N	N	N	N	W	N	N
1980	N	N	N	N	N	N	N	N	N	N	N	N	D	N	N	N	N	N
1981	N	N	N	N	N	N	N	N	N	N	N	N	N	N	W	D	N	N
1982	N	N	N	N	N	N	N	N	N	VW	VW	VW	W	W	VW	N	N	N
1983	N	W	N	N	N	N	N	W	N	N	N	N	D	D	D	VP	N	VP
1984	N	N	N	N	W	N	N	N	N	N	N	N	N	N	N	N	N	N
1985	N	W	W	N	N	N	N	N	N	N	N	N	N	N	N	W	VW	W
1986	N	N	N	N	N	N	N	N	N	N	N	N	VW	N	N	VW	N	N
1987	N	N	N	N	N	N	N	W	N	VW	VW	VW	D	D	D	N	N	N
1988	N	N	N	N	N	N	N	N	N	N	N	N	D	N	N	N	W	N
1989	N	N	N	N	N	N	N	N	N	N	N	N	VW	N	N	N	N	N
1990	N	N	N	N	N	N	N	N	N	N	N	N	D	N	N	D	N	N
1991	N	N	N	N	N	N	N	N	N	N	N	N	D	N	N	W	N	N
1992	N	N	N	N	N	N	N	N	N	N	N	N	D	N	D	VW	N	N
1993	N	N	N	N	N	N	N	N	N	N	N	W	N	N	N	VP	N	N
1994	N	W	W	VW	W	VW	VW	W	VW	N	N	VW	VW	W	W	W	W	N
1995	N	N	N	N	N	N	N	N	N	VW	N	N	D	N	N	W	N	N
1996	N	N	N	VW	VW	W	N	N	N	N	N	N	D	N	D	VP	D	N
1997	N	N	N	N	N	N	N	N	N	N	W	N	N	N	N	N	N	D
1998	VW	N	N	N	W	W	N	N	N	N	N	N	D	D	D	VP	N	D
1999	N	N	N	N	N	N	N	N	N	N	N	N	D	D	D	D	W	N
2000	N	N	N	N	N	N	N	N	N	N	N	N	VW	N	N	N	N	N
2001	N	N	N	N	N	N	N	N	N	N	W	N	N	N	N	VW	N	W
2002	N	N	N	N	N	N	N	N	N	N	W	N	D	D	D	D	N	N
2003	N	N	N	VW	W	VW	N	N	N	N	N	N	N	N	D	N	N	N
2004	N	N	N	N	N	N	N	N	N	N	N	W	N	N	N	VW	VW	VW
2005	N	N	N	N	W	VW	N	N	N	N	N	N	VW	W	VW	N	D	N
2006	N	N	N	W	N	N	N	N	N	N	N	N	N	N	N	N	D	N
2007	N	N	N	N	N	N	N	N	N	N	W	N	D	N	N	D	N	N
2008	N	N	N	N	N	N	VW	N	N	VW	N	N	N	D	D	VP	D	N
2009	N	N	N	N	N	N	N	N	N	N	N	N	N	N	N	D	N	N

Ob: Observed Re: Regression NN: Neural Network VW: Very Wet W: Wet N: Normal D: Dry VD: Very Dry.

HESSD
10, 13333–13361, 2013

Table 9. Evaluation on the predicted results of the regression model and ANN model.

Factor\Method	R^2		RMSE		Nash–Sutcliffe		Accuracy		Heidke Skill Score		Trend Accuracy	
Month	Reg	ANN	Reg	ANN	Reg	ANN	Reg	ANN	Reg	ANN	Reg	ANN
Jan	× 0.218	√ 0.313	× 0.18	√ 0.17	× 0.22	√ 0.31	× 40 %	√ 47 %	× 8 %	√ 21 %	√ 81 %	√ 81 %
Feb	× 0.243	√ 0.263	× 0.23	√ 0.23	× 0.24	√ 0.26	× 37 %	√ 51 %	× 4 %	√ 24 %	√ 69 %	× 67 %
Mar	√ 0.336	× 0.287	√ 0.19	× 0.20	√ 0.34	× 0.28	× 28 %	√ 35 %	× 7 %	√ 12 %	√ 81 %	√ 81 %
Apr	× 0.389	√ 0.536	× 0.19	√ 0.17	× 0.39	√ 0.54	√ 42 %	× 37 %	√ 20 %	× 14 %	√ 81 %	× 79 %
May	√ 0.371	× 0.274	√ 0.20	× 0.22	√ 0.36	× 0.26	√ 49 %	× 47 %	√ 22 %	× 15 %	× 64 %	√ 71 %
Jun	× 0.437	√ 0.513	× 0.17	√ 0.15	× 0.41	√ 0.50	× 91 %	√ 93 %	× 52 %	√ 54 %	√ 21 %	× 19 %
Jul	× 0.298	√ 0.482	× 0.17	√ 0.15	× 0.27	√ 0.47	× 84 %	√ 88 %	× 25 %	√ 40 %	√ 43 %	× 40 %
Aug	× 0.356	√ 0.494	× 0.17	√ 0.14	× 0.32	√ 0.49	× 86 %	√ 91 %	× 45 %	√ 60 %	× 43 %	√ 50 %
Sep	× 0.178	√ 0.761	× 0.15	√ 0.08	× 0.17	√ 0.75	× 88 %	√ 95 %	× 13 %	√ 48 %	√ 12 %	× 10 %
Oct	× 0.281	√ 0.447	× 0.17	√ 0.14	× 0.27	√ 0.44	× 81 %	√ 86 %	× 32 %	√ 48 %	× 43 %	√ 55 %
Nov	× 0.331	√ 0.367	× 0.19	√ 0.18	× 0.32	√ 0.37	× 44 %	√ 51 %	× 18 %	√ 27 %	√ 86 %	√ 86 %
Dec	× 0.253	√ 0.341	× 0.19	√ 0.18	× 0.25	√ 0.34	× 35 %	√ 42 %	× 5 %	√ 11 %	× 71 %	√ 81 %

√ acceptable.
× unacceptable.

HESSD
10, 13333–13361, 2013

Title Page
Abstract | Introduction
Conclusions | References
Tables | Figures
◂ | ▸
Back | Close
Full Screen / Esc
Printer-friendly Version
Interactive Discussion

Table A1. Rainfall categories base on SPI index.

SPI Value	Rainfall category
SPI <−100	very dry
− 100 ≤ SPI < −50	dry
−50 ≤ SPI ≤ 50	normal
50 ≤ SPI < 100	wet
100 ≤ SPI	very wet

HESSD

10, 13333–13361, 2013

Drought forecasting by atmospheric circulation factors

S. K. Sigaroodi et al.

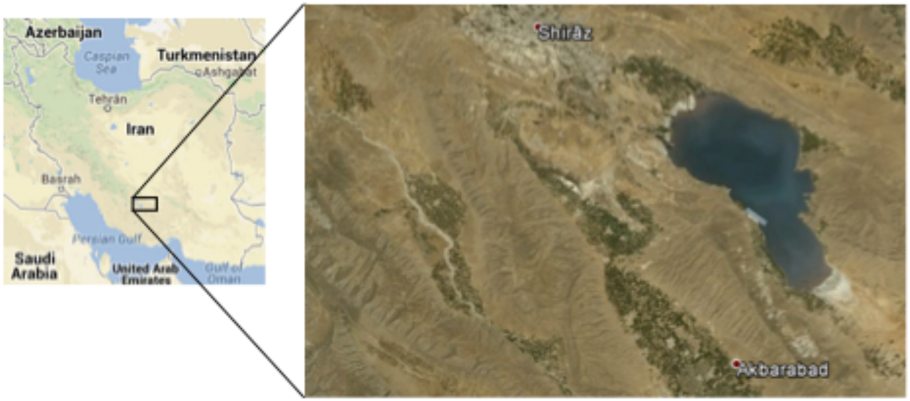

Fig. 1. Satellite image of Maharloo Lake in the southern Iran.

HESSD
10, 13333–13361, 2013

Drought forecasting by atmospheric circulation factors

S. K. Sigaroodi et al.

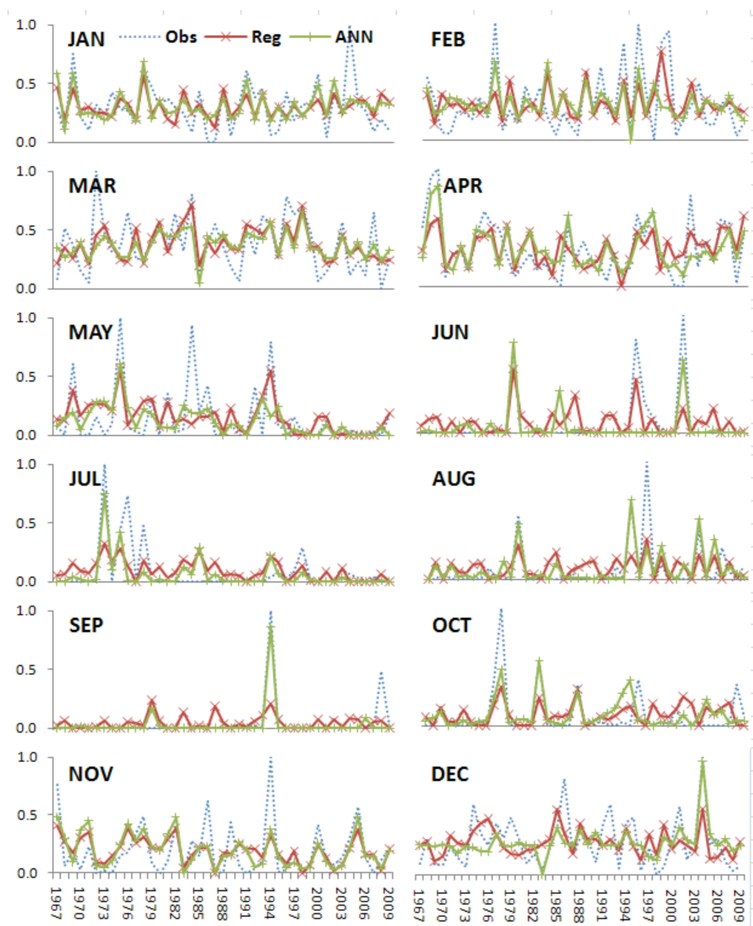

Fig. 2. Comparisons between observations and ANN model results as well as regression model results (normalized precipitations are shown on the vertical axis).

HESSD
10, 13333–13361, 2013

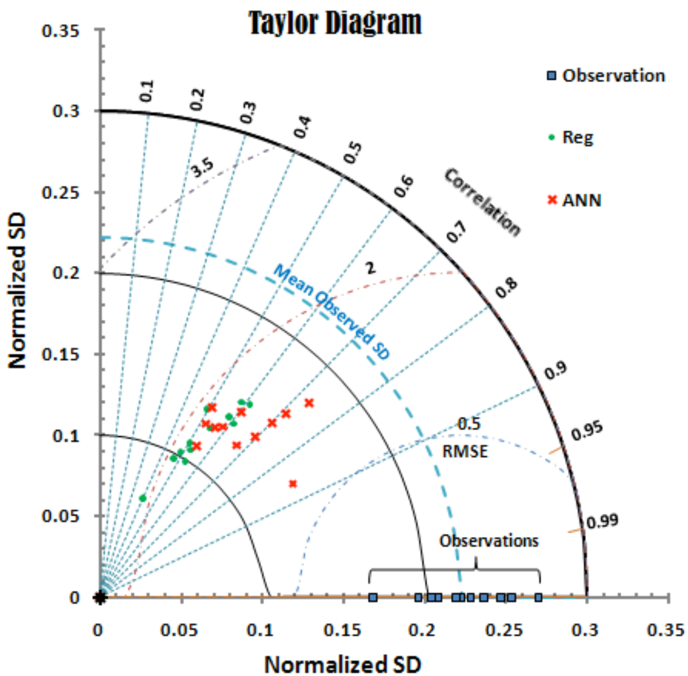

Fig. 3. Scatter plot of the predicted data of the regression and ANN models on a Taylor diagram.

HESSD
10, 13333–13361, 2013

Drought forecasting by atmospheric circulation factors

S. K. Sigaroodi et al.